Supporting Information

Cyclotriphosphazene-based Organic Frameworks as Third-order Nonlinear Optical Materials

Suresh Bommakanti,[a,†] Satyapriya Nath,[a,c,†] Rudrashish Panda,[b] Ritwick Das*[b,c,e] and Bishnu P. Biswal*[a,c,d]

[a]*School of Chemical Sciences, National Institute of Science Education and Research Bhubaneswar, Jatni, Khurda, Odisha, 752050, INDIA*

[b]*School of Physical Sciences, National Institute of Science Education and Research Bhubaneswar, Jatni, Khurda, Odisha, 752050, INDIA*

[c]*Homi Bhabha National Institute, Training School Complex, Anushakti Nagar, Mumbai, 400094, INDIA*

[d]*Centre for Interdisciplinary Sciences, National Institute of Science Education and Research Bhubaneswar, Jatni, Khurda, Odisha, 752050, INDIA*

[e]*Optics and Photonics Centre, Indian Institute of Technology Delhi, Hauz Khas, New Delhi 110 016, India*

[†] *S.B. and S.N. contributed equally to this work.*

**Email:* ritwick.das@niser.ac.in; bp.biswal@niser.ac.in

Table of Contents

Section S-1: Materials and Instrumentation

Materials

All the chemicals and solvents were received as reagent grade and used without further purification except that the aldehyde monomer, hexa(4-formyl-phenoxy)cyclotriphosphazene (CTP-6-CHO), was synthesised using a previously reported literature protocol.[1] The starting materials for CTP-6-CHO and other monomers used to synthesise the frameworks were commercially available and purchased from Sigma-Aldrich, BLDpharm and TCI chemicals, depending upon their availability.

General instrumentation and methods:

Powder X-ray diffraction (PXRD) patterns were collected on a Bruker D8 Advance X-ray powder diffractometer with Cu Kα radiation (λ = 1.5418 Å) in Debye-Scherrer geometry at room temperature.

Crystal structure modelling. Molecular modelling of the frameworks was carried out using the BIOVIA Materials Studio suite, and the structure and unit cell parameters were relaxed using force fields (Forcite, universal force fields with Ewald electrostatic and van der Waals summations method). The unit cell parameters of the experimentally obtained PXRD patterns were compared with simulated patterns obtained from structural modelling.

Fourier transform infrared (FT-IR) spectra were recorded in an attenuated total reflection (ATR) geometry on a PerkinElmer FT-IR spectrometer with a diamond crystal. The FT-IR spectra were background corrected and collected in the 4000-500 cm^{-1} range. Finally, the data were reported with a wave number (cm^{-1}) scale.

N_2 Sorption analyses were performed at 77 K on a Quantachrome Instruments Autosorb iQ automatic volumetric instrument. All the samples were outgassed for 12 h at 150 °C under the vacuum before the gas adsorption studies. The surface areas were evaluated using the Brunauer-Emmett-Teller (BET) model applied between P/P_0 values of 0.05 and 0.3.

Solid-state NMR spectra (ssNMR) were recorded on a Bruker Advance III 400 MHz spectrometer (magnetic field 9.4 T). The samples were packed in 4 mm ZrO_2 rotors and spun in a Bruker WVT BL4 double resonance MAS probe. The chemical shift was referenced relative to tetramethyl silane (^{13}C) as an external standard. The spinning rate was 12.5 kHz. A standard cross-polarisation sequence with a 2 ms ramped contact pulse was used for ^{13}C, and

4K scans were routinely accumulated. Carbon chemical shifts are expressed in parts per million (δ scale).

Thermogravimetric analyses (TGA) were carried out on a TG50 analyser (Mettler-Toledo) and an SDT Q600 TG-DTA analyser in an N_2 atmosphere at a heating rate of 10 ºC min^{-1} within a temperature range of 40 − 900 °C.

UV-visible absorption spectra: Solid-state UV-visible spectra [diffuse reflectance spectra (DRS)] were collected on a UV−2600 Shimadzu UV−visible spectrophotometer (referenced to barium sulfate) at room temperature. Absorption spectra were calculated from the reflectance data using the Kubelka-Munk function.

Solution UV-visible spectra were recorded by dispersing the materials in 2-propanol (conc. 1 mg/1 mL), and the measurements were carried out in a 3 mL quartz cuvette with an optical path length of 1 cm.

Steady-state fluorescence measurements were carried out on a Cary Eclipse fluorescence spectrophotometer (Agilent Technologies), and the average decay time of the fluorescence species was measured using a time-correlated single photon counting (TCSPC) spectrometer (Edinburgh, model OB920) with a 374 nm laser as excitation sources.

Scanning electron microscopy (SEM) measurements were executed with a Merlin Compact field effect SEM (FESEM) with a GEMINI-I electron column, Zeiss Pvt. Ltd., Germany. The samples were prepared by sonicating the materials in 2-propanol for 30 min, drop-casted on silicon wafers and sputtered with Pt to examine their morphologies.

Transmission electron microscopy (TEM) images were captured by a JEOL microscope (JEM-2100) operating at an accelerating voltage of 200 kV. The samples were prepared dry on a carbon-coated copper grid (purchased from Sigma) by drop-casting the dilute suspension of materials in 2-propanol.

Cyclic voltammetry (CV) measurement: CV measurements were performed on a CHI760E electrochemical workstation using a traditional three-electrode set-up in a non-aqueous medium.

Z-Scan technique: Femtosecond laser (fs) pulses from a Yb-doped pulsed fiber laser emitting at 370 fs time scale was employed as an excitation source for the open-aperture (OA) and closed aperture (CA) Z-scan experiments. The central wavelength of the laser was 1030 nm, and the laser pulse repetition rate was fixed to 1 kHz. Using a plano-convex lens of 100 mm

focal length, the beam spot size is approximately 32 μm. The optical power incident on the sample is controlled by a variable attenuator constructed using a half-wave plate and polarising beam-splitter. In order to perform the Z-scan experiment, the sample is translated along the laser beam path (about the focal point of the lens) using a motorised translation stage for a distance of approximately 10 cm. The OA transmittance of the samples in the dispersion state is recorded using two photodetectors, and the recorded data was post-processed in the PC to obtain the normalised transmittance. The CA transmittance measurements are carried out by putting an aperture in front of the detector.

Section S-2: Synthetic Procedures

Synthesis of CTP-TAPB:

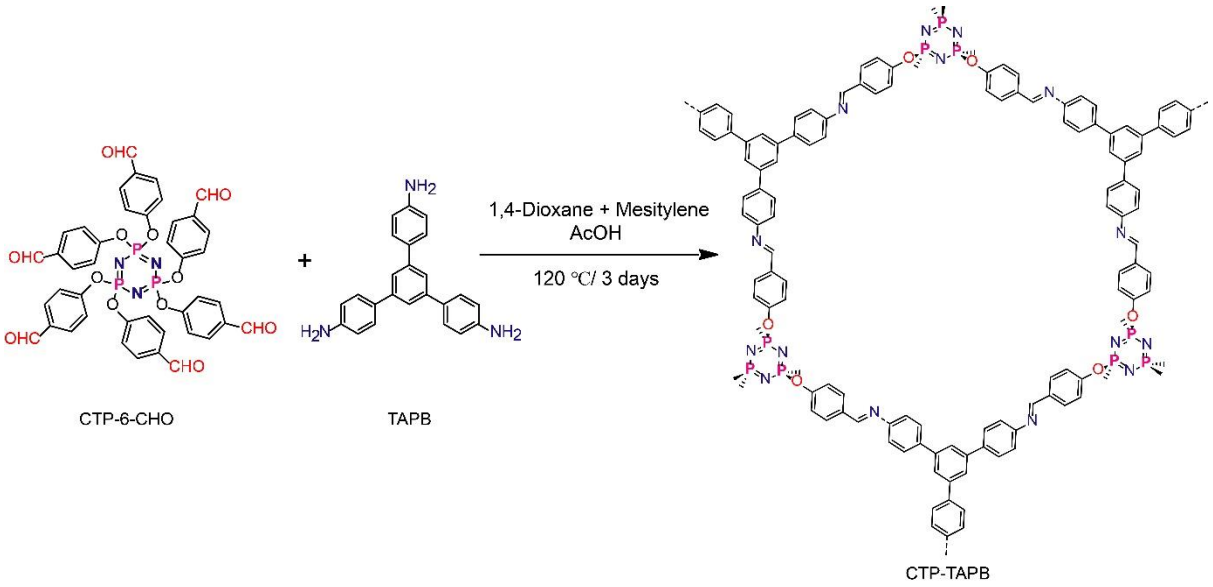

Scheme S1: Schematic representation of the synthesis of **CTP-TAPB**.

[1 mL 1,4-dioxane and mesitylene mixture (4:1, v/v); 0.1 mL aqueous acetic acid (AcOH) solution (6 M)].

The **CTP-TAPB** was synthesised by Schiff base condensation of CTP-6-CHO and 1,3,5- tris-(4-aminophenyl)benzene (TAPB). A Schlenk tube was charged with CTP-6-CHO (10 mg, 0.0116 mmol) and TAPB (8.16 mg, 0.023 mmol). To the above mixture, 1 mL of 1,4-dioxane and mesitylene mixture (4:1, v/v) and 0.1 mL aqueous acetic acid (AcOH) solution (6 M) were added, which is followed by sonication for 5 min to afford a homogenous suspension. Subsequently, the Schlenk tube was fitted with a screw cap and degassed under liquid N_2 (77

K) by three freeze-pump-thaw cycles. The tube was allowed to attain room temperature, and the reaction mixture was heated to 120 ℃ for three days. After the reaction, a tan-yellow solid was collected by filtration and washed with N, N-dimethylacetamide (DMAc), 2-propanol, and acetone. Finally, the purified compound was obtained by Soxhlet extraction in THF for 48 h and then dried at 60 ℃ overnight under vacuum to acquire **CTP-TAPB** in ~72 % yield.

Synthesis of CTP-TCPB:

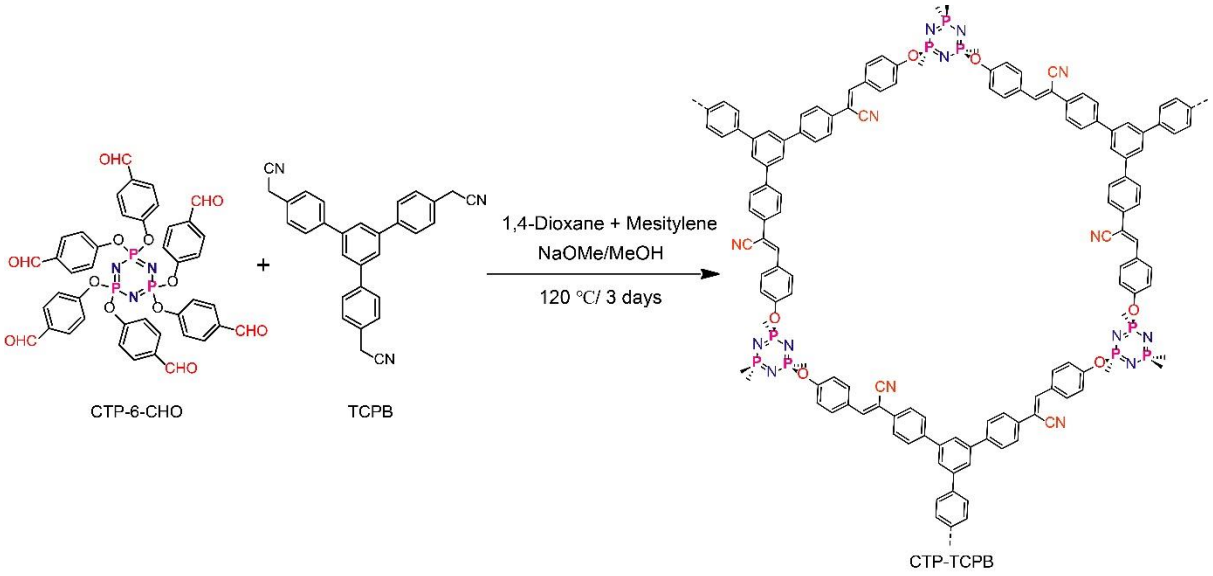

Scheme S2: Schematic representation of the synthesis of **CTP-TCPB**.

[1 mL 1,4-dioxane and mesitylene mixture (4:1, v/v); 1 mL of NaOMe in methanol solution (0.057 M)].

CTP-TCPB was synthesised by a Knoevenagel condensation of CTP-6-CHO and 1,3,5- tris-(4-cyanomethylphenyl)benzene (TCPB). In a Schlenk tube fitted with a screw cap, CTP-6-CHO (10 mg, 0.0116 mmol) and TCPB (9.75 mg, 0.023 mmol) were charged. 1 mL of 1,4-dioxane and mesitylene mixture (4:1, v/v) and 1 mL of NaOMe in methanol solution (0.057 M) were added and sonicated for 5 min to afford homogenous suspensions. Further, the reaction mixture was degassed under liquid N_2 (77 K) by three freeze-pump-thaw cycles; then, the tube was vacuum sealed. After attaining room temperature, the reaction mixture was heated to 120 ℃ for three days. A yellow solid was collected by filtration and washed with N, N-dimethylacetamide (DMAc), 2-propanol, and acetone. The final framework material was purified by Soxhlet extraction in THF for 48 h and then dried at 60 ℃ overnight under vacuum to obtain **CTP-TCPB** in ~75 % yield.

Section S-3: Powder X-ray Diffraction and Structural Analysis

The CTP-6-CHO monomer employed in the construction of these frameworks possesses a unique structural configuration, featuring six cross-sided arms outside the central plane, which serves as the node module for the synthesised materials (Figure 1, main manuscript). The distinctive stereoscopic structure of CTP-6-CHO is characterised by an O-P-O plane that is perpendicular to the aromatic ring plane of the cyclotriphosphazene (N3P3 ring). This configuration imparts non-traditional 2D planarity to the as-prepared frameworks. To achieve the assembly of frameworks with an ordered long-range structure, CTP-6-CHO interacts with C3-symmetric linkers (TAPB/TCPB), and two side chains anchored at the O-P-O bonds align in parallel. This alignment results in a hetero-pore structure featuring primary hexagonal pores and lateral narrow pores. During the formation of the continuous extended framework structure, the N3P3 plane undergoes lateral rotation relative to the P-O-P plane due to stretching effects and spatial limitations. However, owing to the inherent 3D structural characteristics of pentavalent phosphorus and the presence of spatial steric hindrance, it is unfeasible for the two planes to align perfectly, leading to the emergence of a unique "quasi-3D" structure that incorporates elements of both two and three dimensions, yielding 2D frameworks with 3D structural attributes. Thus, the intricate nature of the CTP-monomer's structure necessitates a specific molecular arrangement that negatively affects the packing between the successive COF layers, resulting in low crystallinity and low porosity in these materials.

The crystallinity of the synthesised frameworks was analysed by recording the power X-ray diffraction (PXRD) studies. Both CTP-TAPB and CTP-TCPB exhibit low to moderate crystallinity. In addition, the structures were modelled using the Material Studio (MS) software. In contrast to the expected 2D COF structure, the CTP-containing frameworks exhibit unique structural features owing to the inherent 3D stereotypic characteristics of the pentavalent phosphorus atoms. For this reason, the side arm of the O-P-O bond deviates from the planar (2D) structure, resulting in quasi-3D structures.[1] Besides, two different types of arrangement of the side chains are responsible: Type-I and Type-II. In type I, the CTP core acts as a C3 symmetric linker with two arms of the phosphorous atoms leading to hexagonal structures, whereas in type II, the CTP core acts as a C6 linker, resulting in wheel-shaped structures. In the present work, the CTP-core adopts the C3 symmetry, thus yielding the hexagonal-type architecture for both frameworks.

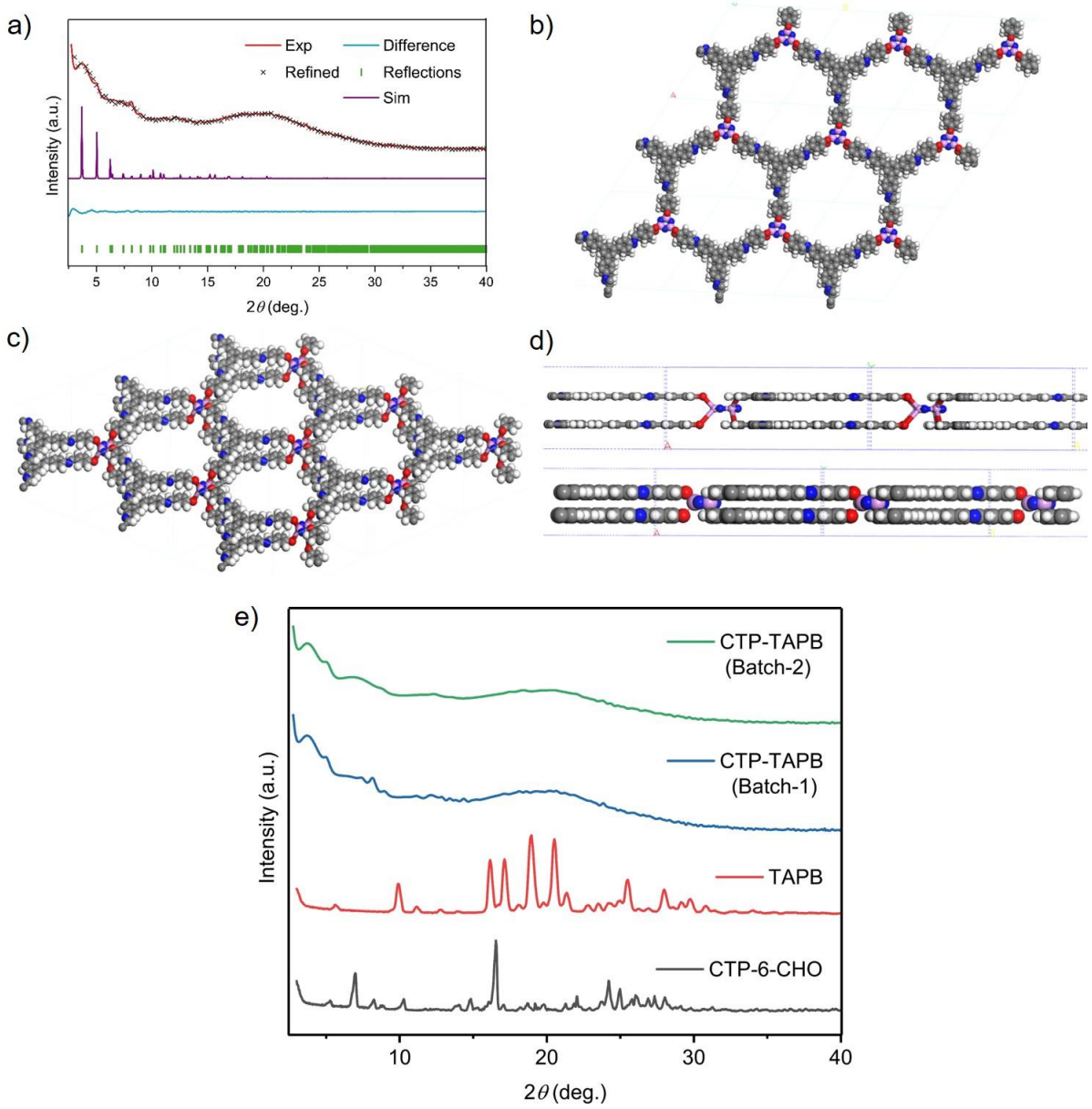

Figure S1. PXRD and structural modelling of **CTP-TAPB**. a) PXRD and Pawley refinement of **CTP-TAPB** framework. Experimental patterns (red), refined patterns (black), the difference between experimental and refined patterns (cyan), Bragg reflections (green) and simulated AA-stacking pattern (purple) [final Rwp = 4.24% and Rp = 2.99%], b) and c) Structural representations of **CTP-TAPB** with corresponding d) side views of the AA stacking models (P, pink; C, grey; N, blue; O, red; H, white), e) A comparison of PXRD data of monomers (CTP-6-CHO and TAPB), **CTP-TAPB** frameworks synthesised in different batches.

The lattice of **CTP-TAPB** was assigned with optimized cell parameters of a = 19.98, b = 19.99, and c = 9.95 Å; α = 91.53, β = 90.16, and γ = 119.74°.

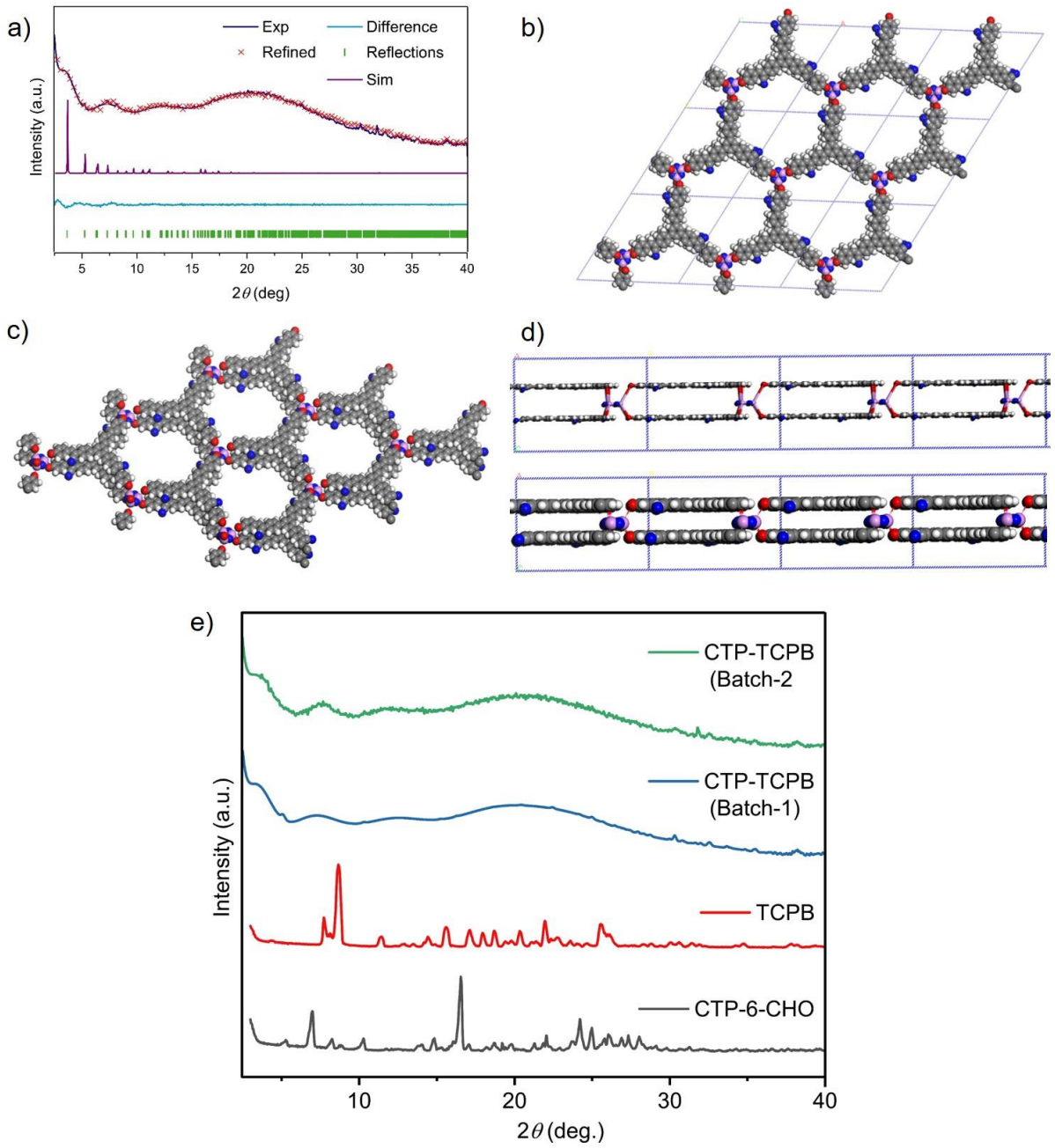

Figure S2. PXRD and structural modelling of **CTP-TCPB**. a) PXRD and Pawley refinement of **CTP-TCPB** framework. Experimental patterns (black), refined patterns (red), the difference between experimental and refined patterns (cyan), Bragg reflections (green) and simulated AA-stacking pattern (purple) [final Rwp = 3.83% and Rp = 2.57%], b) and c) Structural representations of **CTP-TAPB** with corresponding d) side views of the AA stacking models (P, pink; C, grey; N, blue; O, red; H, white), e) A comparison of PXRD data of monomers (CTP-6-CHO and TCPB), **CTP-TCPB** frameworks synthesised in different batches.

The lattice of **CTP-TCPB** was assigned with optimized cell parameters of a = 19.95, b = 19.94, and c = 9.99 Å; α = 90.33, β = 89.87, γ = 119.16°.

Section S-4: FT-IR Spectra

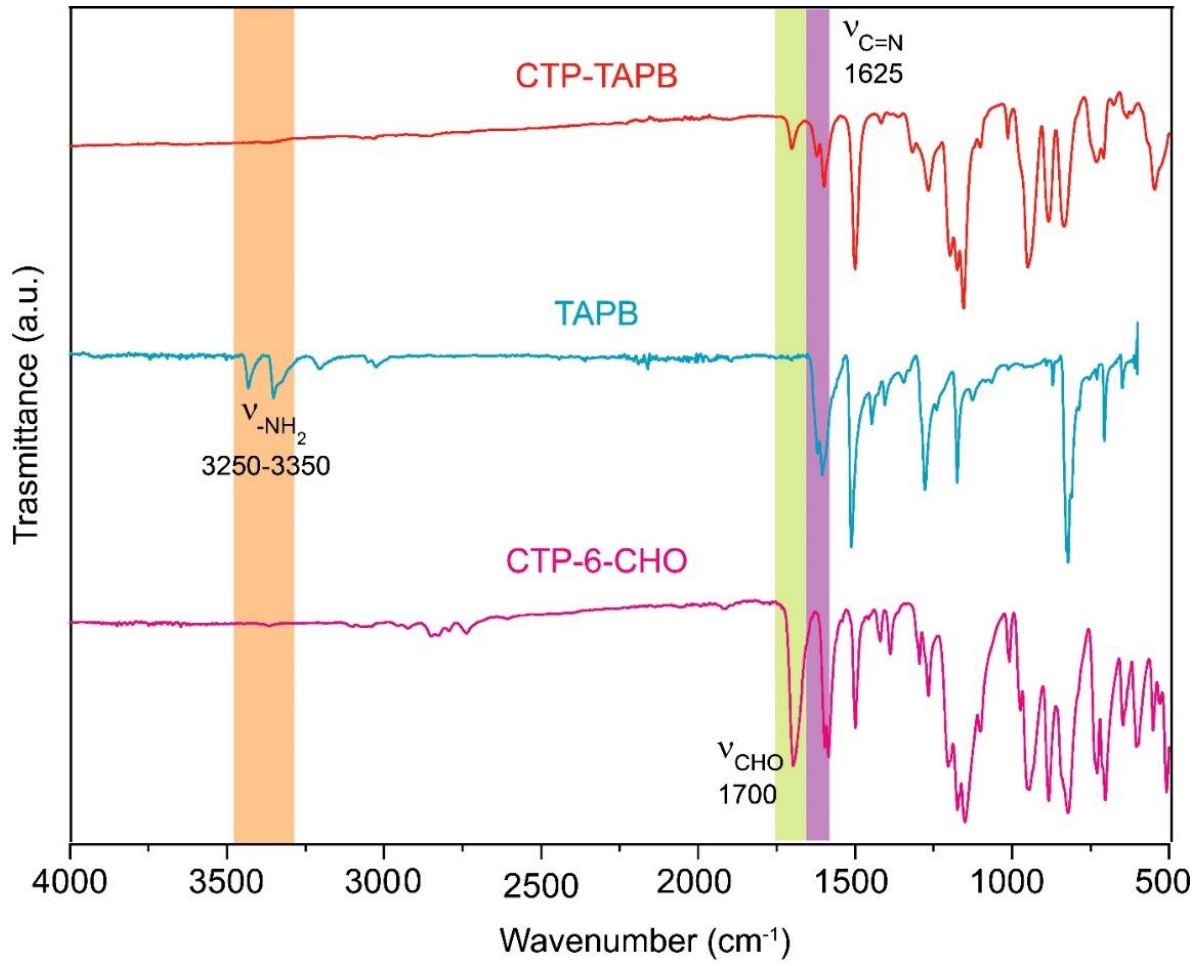

Figure S3. FT-IR spectra of CTP-6-CHO, TAPB, and **CTP-TAPB**.

The successful polymerisation of CTP-6-CHO and 1,3,5-tris(4-aminophenyl)benzene (TAPB) has been analysed by FT-IR spectroscopy. The attenuation of C=O stretching frequency at 1700 cm^{-1} and N-H stretching bands in the range of 3250 - 3350 cm^{-1} corresponding to CTP-6-CHO and TAPB, respectively, confirms the Schiff-base polymerisation between the aldehyde and amine monomers. Further, this is corroborated by the emergence of the new IR band at 1625 cm^{-1} corresponding to the C=N stretching frequency confirming imine bond formation in **CTP-TAPB**.

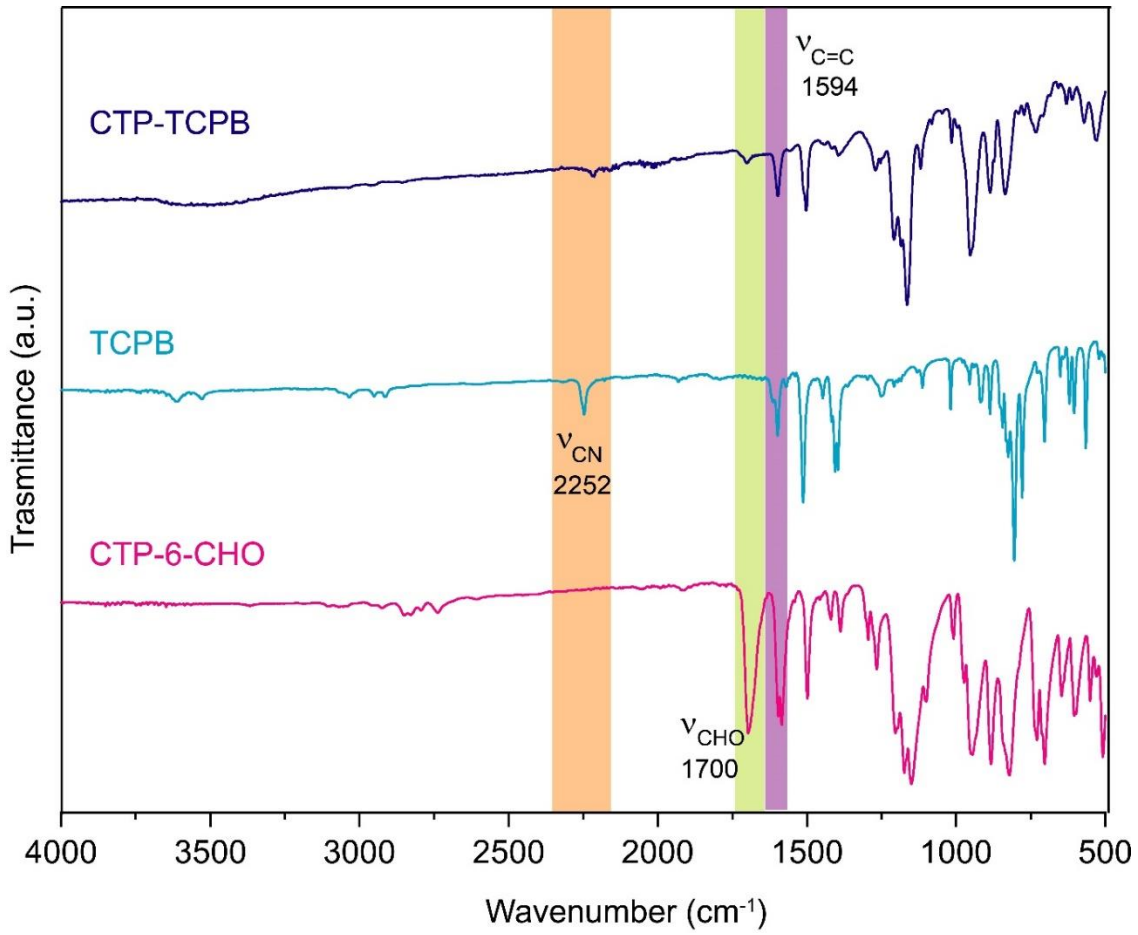

Figure S4. FT-IR spectra of CTP-6-CHO, TCPB, and **CTP-TCPB**.

The Knoevenagel polymerisation of hexa(4-formyl-phenoxy)cyclotriphosphazene (CTP-6-CHO) and 1,3,5-tris(4-cyanomethylphenyl)benzene has been analysed by FT-IR spectroscopy. The attenuation of the C=O stretching frequency at 1700 cm^{-1} confirms the successful polymerisation between the aldehyde and TCPB monomers. Further, this is corroborated by the emergence of the new IR band at 1594 cm^{-1} and 2252 cm^{-1} corresponding to the C=C and C≡N stretching frequencies, respectively, confirming the vinylene-linkage formation in **CTP-TCPB**.

Section S-5: Raman Spectra

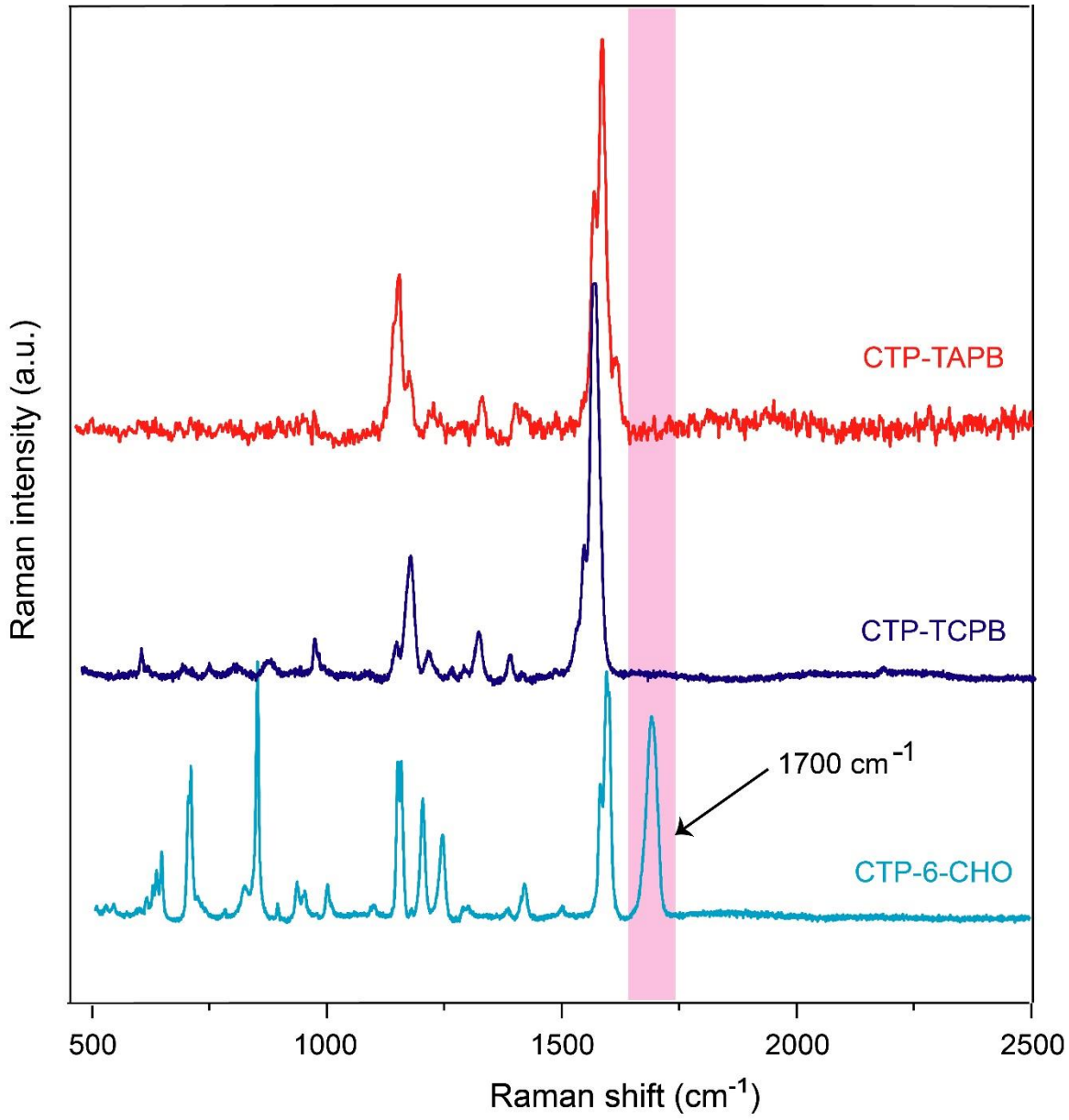

Figure S5. Comparison of Raman spectra of CTP-6-CHO, **CTP-TAPB** and **CTP-TCPB**.

The chemical nature and incorporation of the monomeric units into the frameworks were studied by Raman spectroscopy. The comparison of CTP-6-CHO (aldehyde monomer) and **CTP-TAPB, CTP-TCPB** results that the absence of characteristic Raman shift at 1700 cm^{-1} corresponding to C=O stretching vibration confirms the consumption of the aldehyde functional group in resulting imine and vinylene-linked frameworks.

Section S-6: ^{13}C-CP-MAS Solid-State NMR

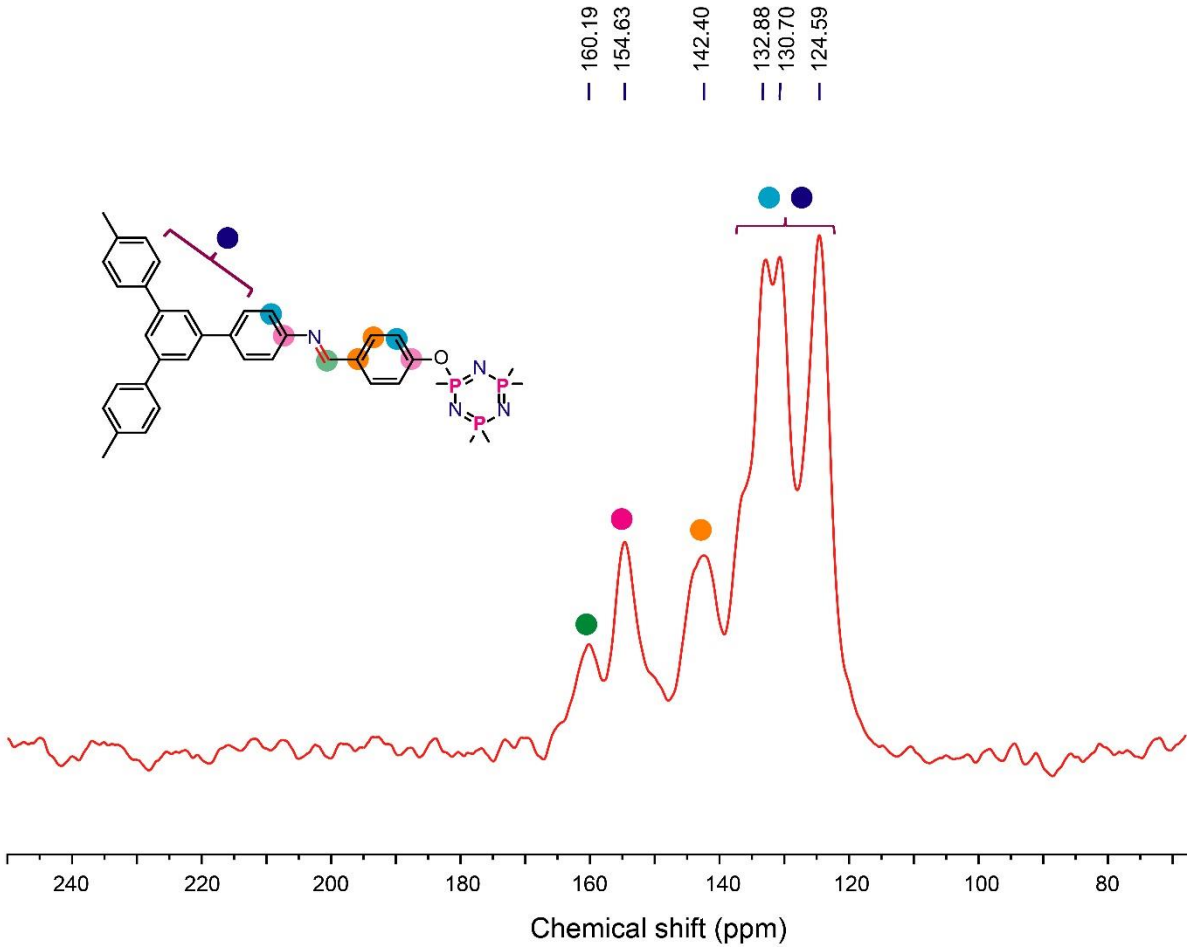

Figure S6. ^{13}C CP-MAS solid-state NMR spectra of **CTP-TAPB**.

To support the structural confirmation of **CTP-TAPB**, we have recorded the CP-MAS-ssNMR. The corresponding ssNMR spectra exhibit resonance peaks at 124.59, 130.70, 132.88, 142.40, 154.63 and 160.19 ppm. The signals in the 124 -142 ppm range were assigned to aromatic carbons of phenyl rings of the **CTP-TAPB** framework. In addition, the peak at 160 ppm corresponding to *C=N imine carbons confirms the successful condensation of CTP-6-CHO and TAPB.

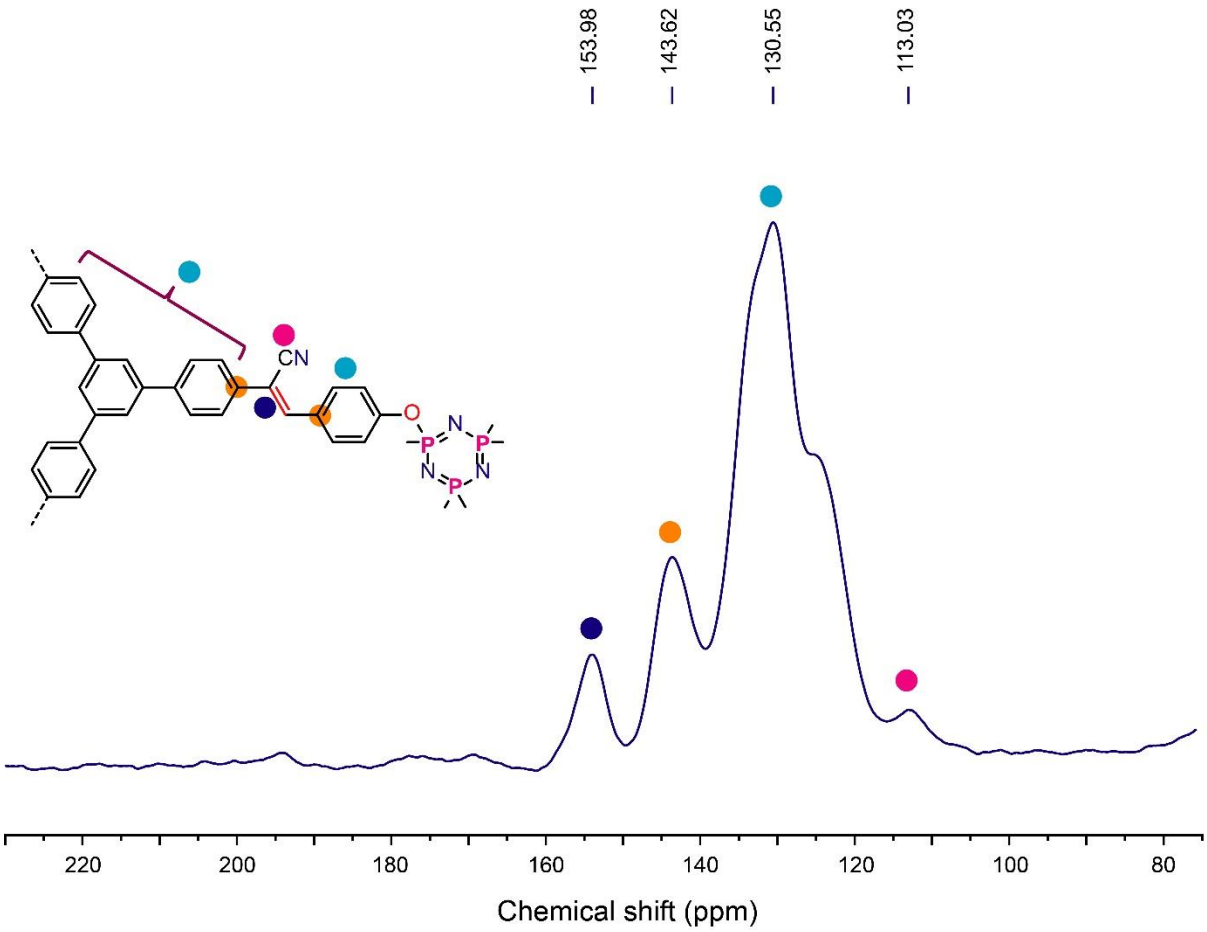

Figure S7. ^{13}C CP-MAS solid-state NMR spectra of **CTP-TCPB**.

The Knoevenagel condensation of CTP-6-CHO and 1,3,5-tris(cyanomethyl)benzene was probed by ^{13}C CP-MAS-ssNMR spectroscopy. The ss-NMR spectra of **CTP-TCPB** exhibit resonance peaks at 113.03, 130.55, 143.62 and 153.98 ppm. The signals at 130 -144 ppm were assigned to aromatic carbons of phenyl rings of the **CTP-TCPB** framework. In addition, the peaks at 113 and 154 ppm corresponding to C≡N carbons and vinylene carbons (C=C) confirm the successful condensation of CTP-6-CHO and TCPB.

Section S-7: N_2 Sorption Analysis at 77 K

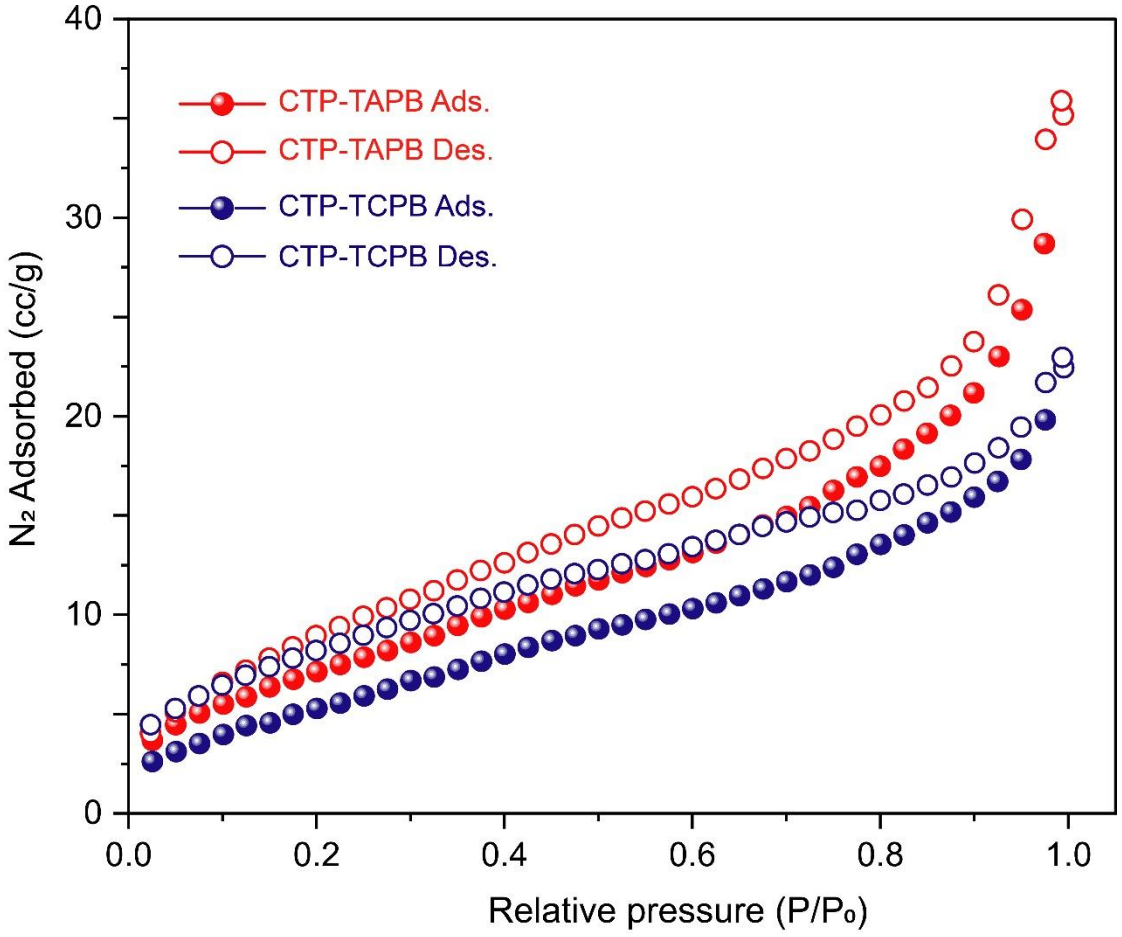

Figure S8. N_2 Sorption analysis of **CTP-TAPB** and **CTP-TCPB** measured at 77 K.

The porosities and the surface area of the **CTP-TAPB** and **CTP-TCPB** were measured using the N_2 adsorption−desorption studies on the activated samples at 77 K in the P/P_o range of 0.0 - 1. Both the frameworks exhibit type-III isotherms with a low N_2 uptake. The Brunauer-Emmett-Teller (BET) surface areas were obtained as 28 $m^2\ g^{-1}$ and 30 $m^2\ g^{-1}$ for **CTP-TAPB** and **CTP-TCPB**, respectively.

Section S-8: Thermal Stability

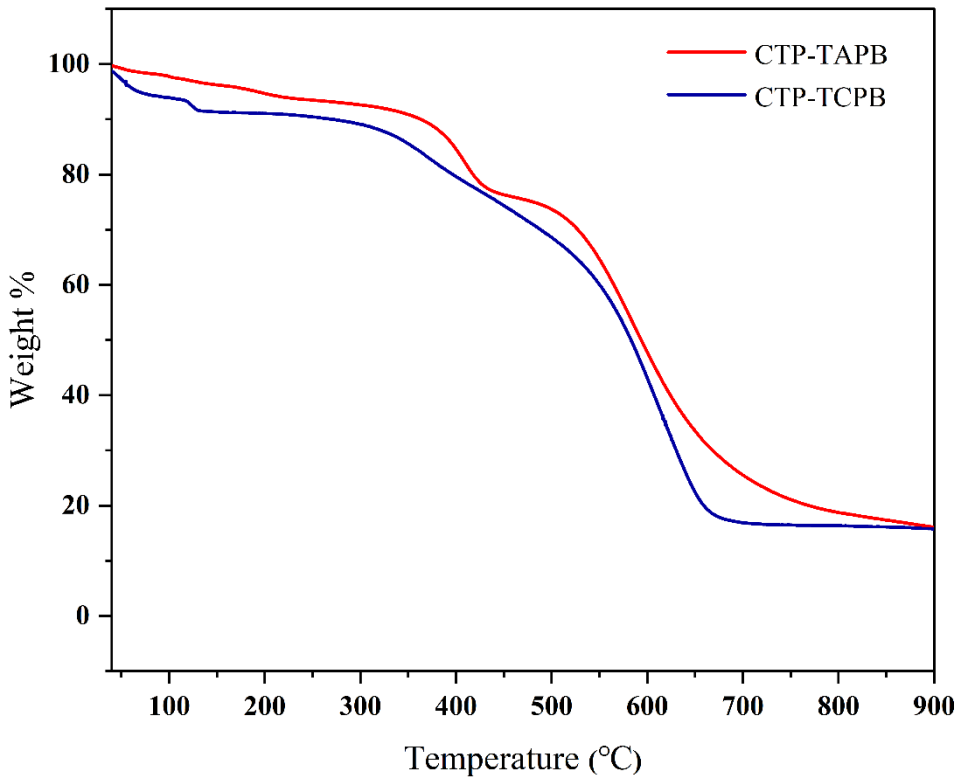

Figure S9: Thermogravimetric analysis (TGA) profiles of **CTP-TAPB** and **CTP-TCPB** frameworks.

The thermal stabilities of the synthesised frameworks were probed by the thermogravimetric analysis (TGA). TGA experiments were performed in an N_2 atmosphere in the range of 40 – 900 °C with a heating rate of 10 °C/min. The TGA profile of **CTP-TAPB** exhibits that this material maintains structural integrity up to 400 °C, whereas **CTP-TCPB** shows stability up to 350 °C. The initial slight weight loss for the **CTP-TAPB** was attributed to the moisture present in the sample. Beyond stipulated stable temperatures, both frameworks undergo continuous weight loss, indicating the structural collapse of the framework backbone.

Section S-9: Scanning Electron Microscopy

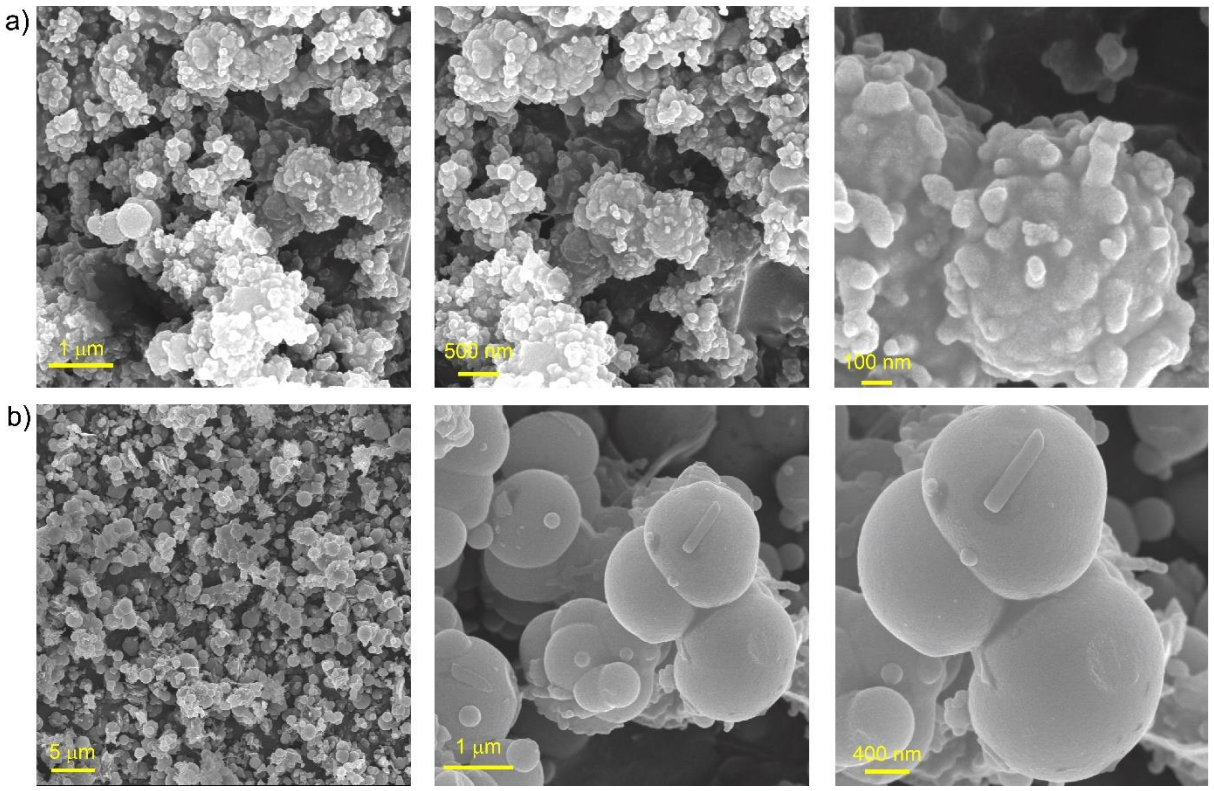

Figure S10. SEM images of a) **CTP-TAPB** and b) **CTP-TCPB**.

The surface morphology of all the synthesised materials was examined by scanning electron microscopy (SEM). The SEM images of the **CTP-TAPB** show spherical morphology with a fibre-type structure on the surface. On the other hand, **CTP-TCPB** exhibits uniform spherical morphology.

Section S-10: Transmission Electron Microscopy

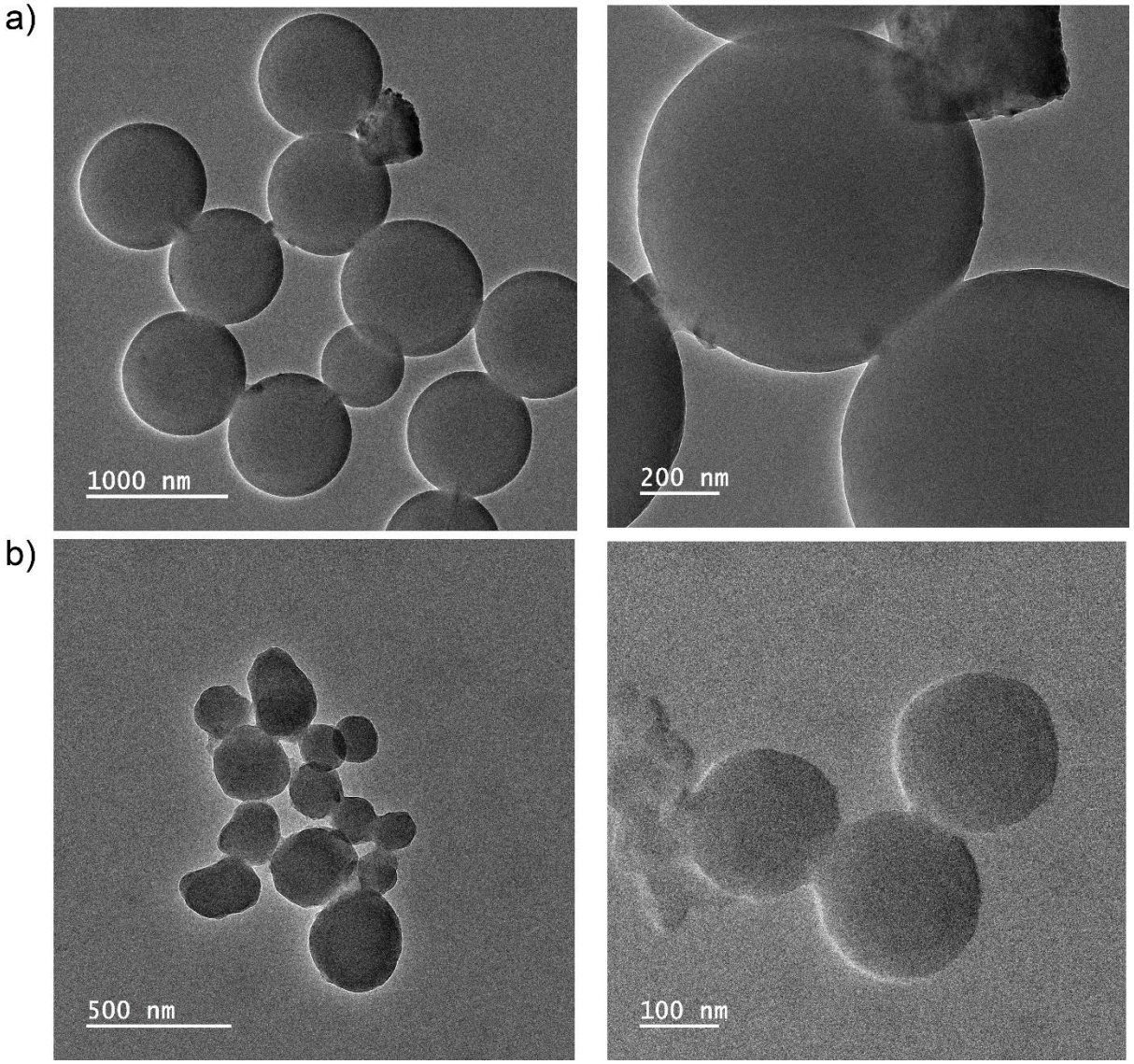

Figure S11. TEM images of a) **CTP-TAPB** and b) **CTP-TCPB**.

The surface morphology of all the synthesised materials was examined by transmission electron microscopy (TEM). The TEM images of the **CTP-TAPB** and **CTP-TCPB** exhibit uniform spherical morphology.

Section S-11: UV-Vis and Photoluminescence (PL) Measurements

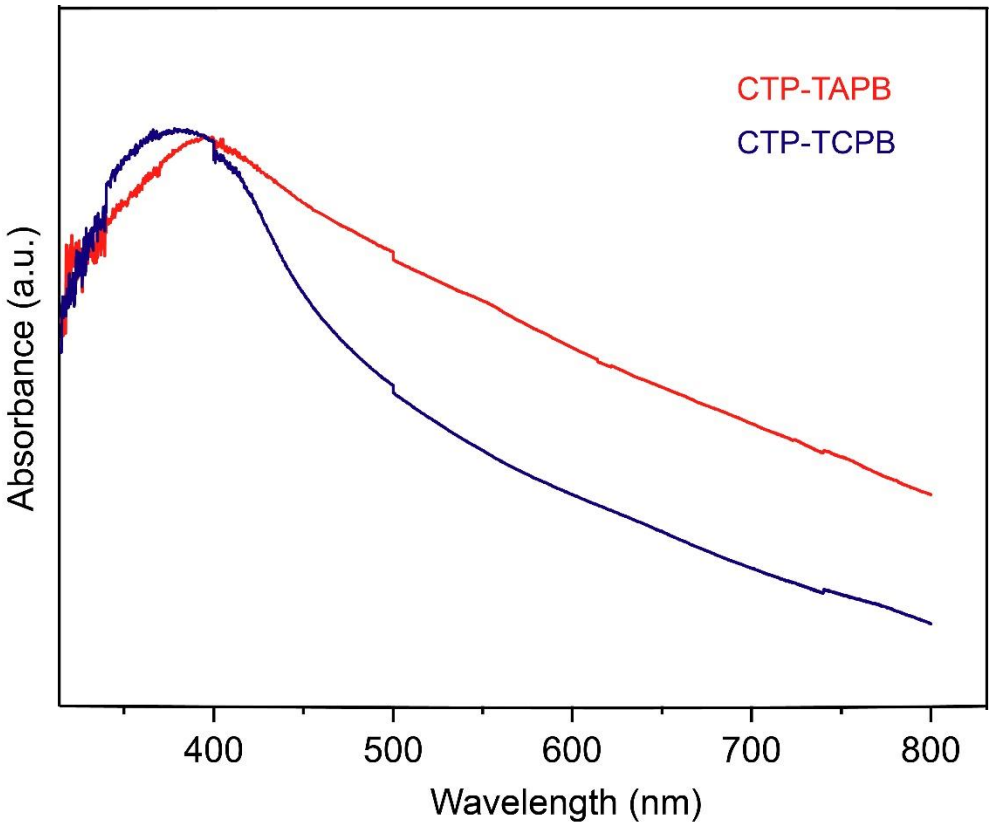

Figure S12. UV-visible absorption spectra of **CTP-TAPB** and **CTP-TCPB** frameworks, measured by dispersing the powdered samples in 2-propanol.

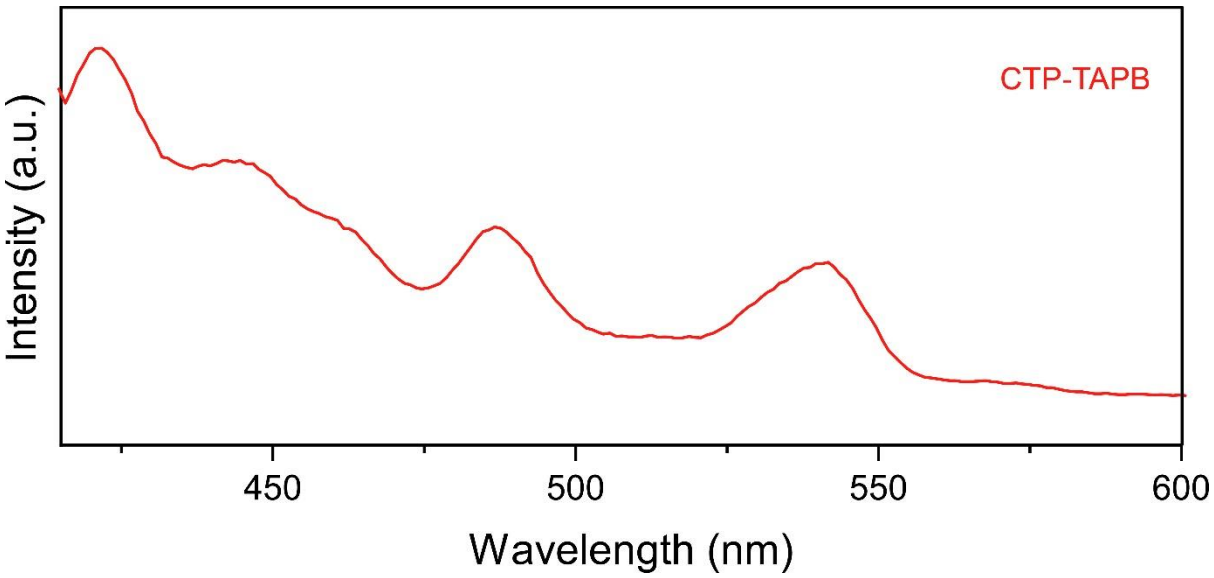

Figure S13. The photoluminescence spectrum of **CTP-TAPB (**measured by dispersing the powdered samples in 2-propanol).

Section S-12: Fluorescence Lifetime Measurements

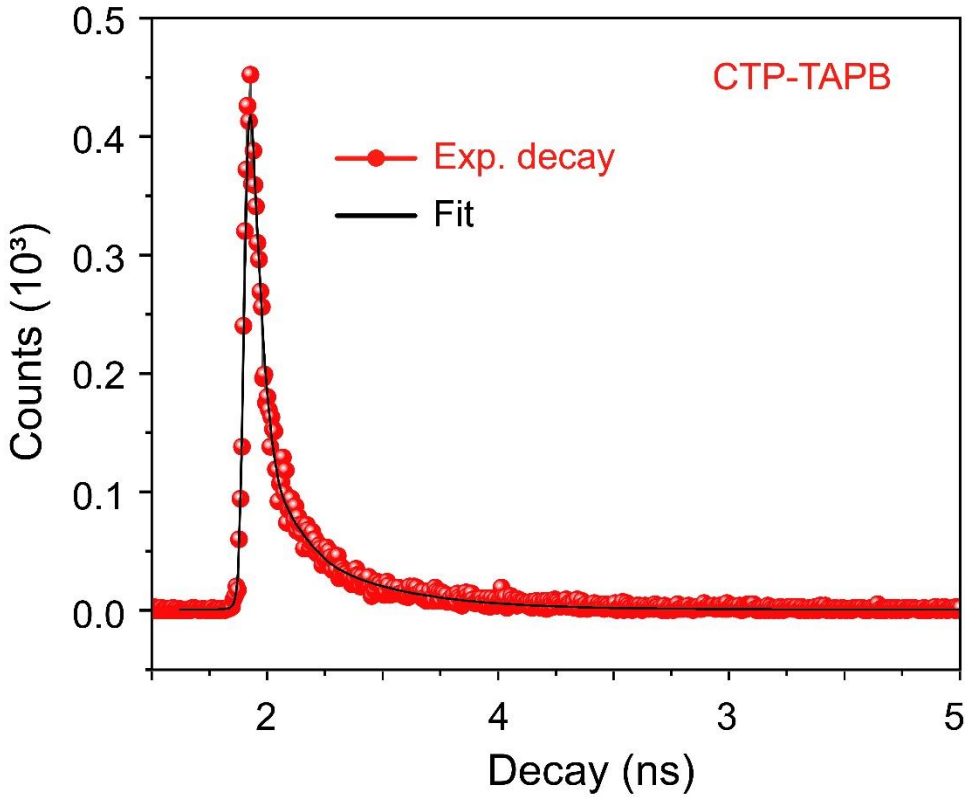

Figure S14. Lifetime measurement of excited-state species using the time-correlated single photon counting (TCSPC) method for **CTP-TAPB** dispersed in 2-propanol.

The experimental decay curve of the **CTP-TAPB** was fitted with (Eq.1)

Fit: $A+B1\exp(-t/\tau1)+B2\exp(-t/\tau2)+B3\exp(-t/\tau3)+B4\exp(-t/\tau4)$ …… Eq. 1

The average excited-state lifetime was estimated using the following expression (Eq. 2).

$$\text{Average life-time} = \frac{(\tau1 \times B1)+(\tau2 \times B2)+(\tau3 \times B3)+(\tau4 \times B4)}{B1 + B2 + B3 + B4} \quad \text{…… Eq. 2}$$

Section S-13: Cyclic Voltammetric Analysis

The positions of the HOMO (Valence Band) and LUMO (Conduction Band) energies were determined by the cyclic voltammetry (CV).[2] The CV studies were performed in a typical three-electrode cell in non-aqueous electrolyte [0.1 M tetrabutylammonium tetrafluoroborate (NBu_4BF_4) in anhydrous acetonitrile] using Pt wire as the counter electrode, Ag/AgCl (0.01 M) as the reference electrode, and glassy carbon drop-casted with the materials act as a working electrode. Before the start of the experiments, the electrolyte solution was purged with nitrogen (N_2) gas for 30 min. The CV plots of **CTP-TAPB** and **CTP-TCPB** show reduction peaks at -0.772 and -0.738 eV, respectively.

The HOMO/LUMO levels are calculated according to the equations:

$E_{LUMO} = -(4.4 + E_{red})$ eV. …… Eq. 3

$E_{HOMO} = E_{LUMO} - E_{gap}$. …… Eq. 4

Table S1. Cyclic voltammetry data and calculation of HOMO and LUMO energy bands for **CTP-TAPB** and **CTP-TCPB**.

Materials	Reduction potential [E_{red} (V)]	LUMO [eV]	Band gap [eV]	HOMO [eV]
CTP-TAPB	-0.772	-3.628	2.94	-6.568
CTP-TCPB	-0.738	-3.662	2.88	-6.542

Section S-14: Nonlinear optical (NLO) properties

Sample preparation for Z-scan measurements: Third-order nonlinear optical properties of **CTP-TAPB** and **CTP-TCPB** frameworks were measured in the dispersion state. The samples for Z-scan transmission measurements were prepared by dispersing 1 mg of the respective material in 10 ml of 2-propanol, followed by sonication for 30 minutes to obtain a homogenous suspension.

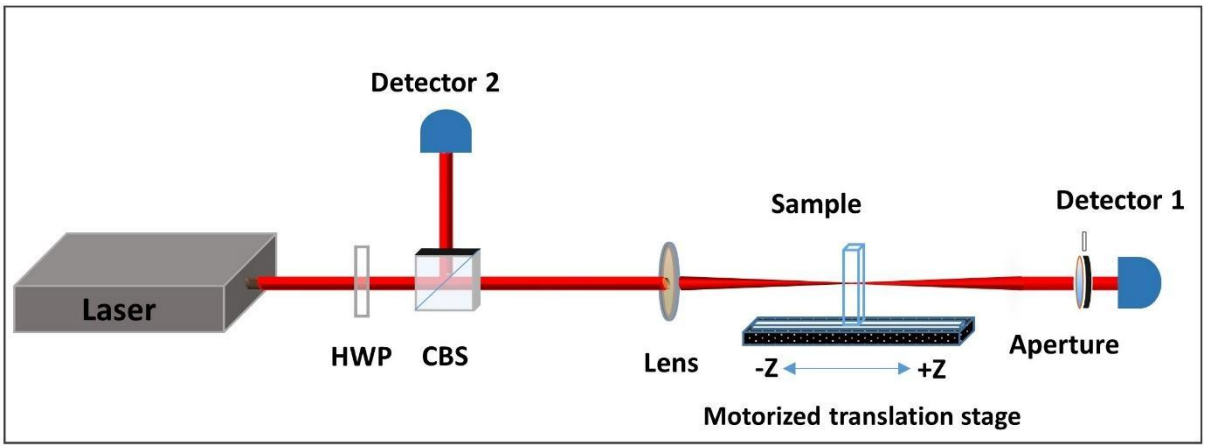

Figure S15. Schematic illustration of the Z-scan set-up used to measure the NLO properties of the synthesised frameworks. (HWP: half-wave plate, CBS: cube beam splitter)

Fig. S15 schematically depicts the Z-scan experimental configuration used for determining the nonlinear absorption (NLA) coefficient (β). A femtosecond Yb-doped fiber laser (Cazadero, M/S Calmar Inc., USA) is employed as an excitation source. The laser delivers a linearly polarised beam in TEM_{00} (Gaussian) mode ($M^2 < 1.05$), having an approximate width of 5 mm. The laser output is in the form of ultrashort pulses of width 370 fs centered at 1030 nm wavelength. The laser repetition rate is kept at 1 kHz for all the Z-scan transmission measurements intended for nonthermal NLO study. The focal spot beam waist radius on the sample is measured to be 32 μm focused using a plano-convex 100 mm focal length lens. A motorised translation stage is used for translating the sample (dispersed solution form) symmetrically through the focal point of the lens over a distance of 10 cm. The incident laser power on the sample is controlled by a combination of a half-wave plate and a polarising beam splitter. The samples (in the dispersed solution form) are mounted on homemade sample holders (cuvette). A pyroelectric photodetector (PD1) is employed to measure the open-aperture (OA) and closed aperture (OA) transmission. In case of closed-aperture (CA)

measurements, a circular aperture of 25% transmittance is placed in front of PD_1. Another pyroelectric photodetector (PD_2) is used to record the fluctuations in the excitation femtosecond laser beam, and the measurements from both photodetectors are simultaneously recorded. The OA Z-scan transmission measurements are calibrated using the standard CS_2 solvent. The samples were prepared in the dispersion state [1 mg of respective material in 10 mL of 2-propanol] for the OA Z-scan transmission measurements.

The NLO signatures of **CTP-TAPB** and **CTP-TCPB** are presented in Fig. S16. The black dots are the experimental observations, and the red solid lines are the theoretical fit to the observed experimental values. In order to quantitatively estimate β, we utilise the dependence of normalised transmittance (T) on β through the relation,[3]

$$T(x) = 1 - \frac{\beta I_0 L_{eff}}{2^{\frac{3}{2}}(1+x^2)} \quad \text{..... (5)}$$

In order to quantitatively estimate the nonlinear refractive index (n_2), we use the following expression to carry out a numerical fitting to the CA transmission,[3]

$$T(x) = 1 - \frac{4\Delta\phi_0 x}{(x^2+9)(x^2+1)} - \frac{2(x^2+3)\Delta\Psi_0}{(x^2+9)(x^2+1)} \quad \text{..... (6)}$$

where,

$L_{eff} = \frac{(1-e^{-\alpha L})}{\alpha}$ is the effective thickness,

α is the linear absorption coefficient, and

I_0 is the on-axis peak intensity at the focal point.

The X-axis in Fig. S17 (a-f) is a normalised propagation distance given by $X=Z/Z_0$, where Z_0 is the Rayleigh length of the laser beam. It is worth noting that Eq. (1) assumes that the sample translation length is sufficiently greater (> 10 times) than that of the Rayleigh length of the Gaussian beam.

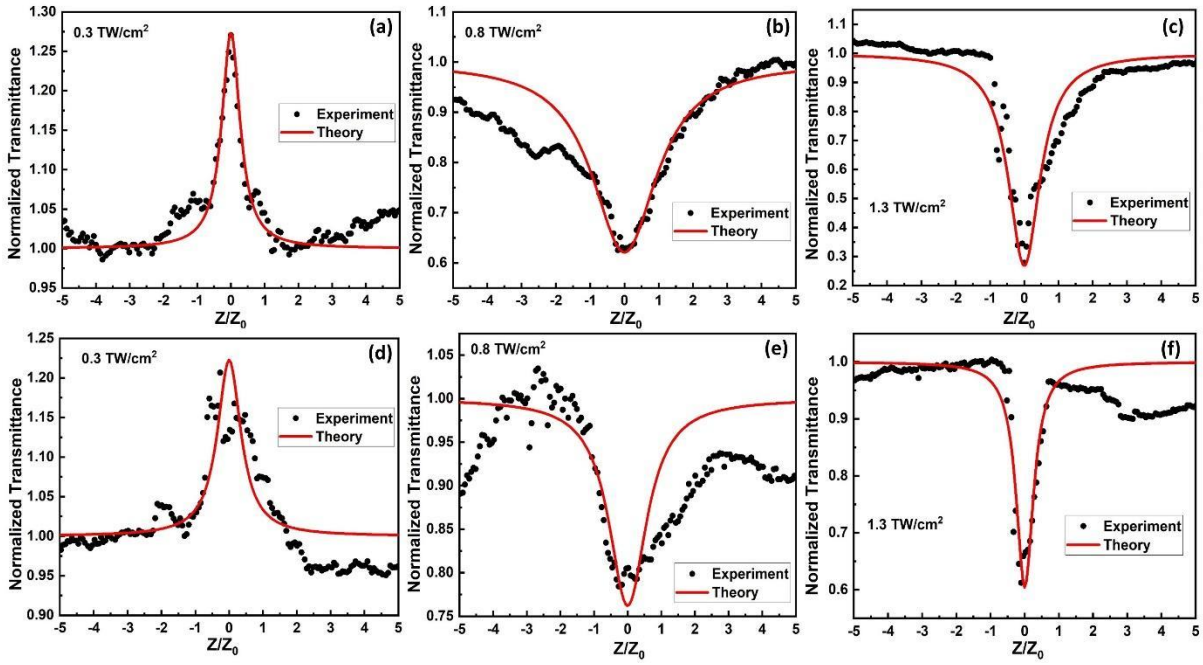

Figure S16. Open aperture Z-scan normalised transmittance curves recorded for (a-c) **CTP-TAPB** and (d-f) **CTP-TCPB** with different incident beam intensities of 0.3 TW/cm^2, 0.8 TW/cm^2 and 1.3 TW/cm^2 using an ultrashort pulsed (370 fs) laser operating at 1 kHz repetition rate.

Table S2. A table presenting the nonlinear absorption coefficient (β) of **CTP-TAPB** and **CTP-TCPB** frameworks, which is measured using an ultrashort pulse (fs) at a repetition rate of 1 kHz and nanosecond (ns) laser (80 kHz repetition rate) centered at a wavelength of 1030 nm and 1064 nm respectively.

Materials	β (cm/GW)	
	370 fs pulse-width at 1 kHz repetition rate (λ = 1030 nm) I_0= 0.3 TW/(cm)^2	1 ns pulse-width at 80 kHz repetition rate (λ = 1064 nm) I_0= 1 MW/(cm)^2
CTP-TAPB	-0.023	-53820
CTP-TCPB	-0.019	-75270

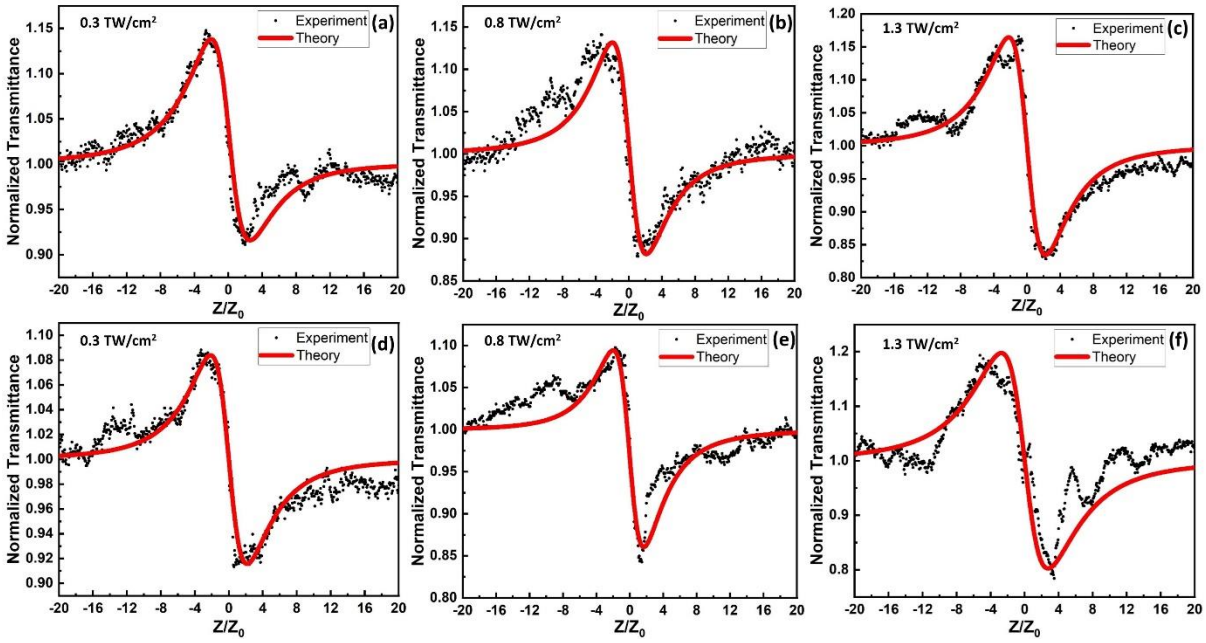

Figure S17. Closed aperture Z-scan normalised transmittance curves recorded for (a-c) **CTP-TAPB** and (d-f) **CTP-TCPB** with different incident beam intensities of 0.3 TW/cm^2, 0.8 TW/cm^2 and 1.3 TW/cm^2 using an ultrashort pulsed (370 fs) laser operating at 1 kHz repetition rate.

The corresponding n_2 values of **CTP-TAPB** and **CTP-TCPB** at the laser intensities of 0.3, 0.8 and 1.3 TW/cm^2 are measured to be -2.12×10^{-7}, -1.2×10^{-7} -1.06×10^{-7}, -1.62×10^{-7}, -1.12×10^{-7} and -1.23×10^{-7} cm^2/GW respectively.

Table S3. A table presenting the nonlinear refractive index (n_2) of **CTP-TAPB** and **CTP-TCPB** frameworks, which are measured using an ultrashort pulse (fs) at a repetition rate of 1 kHz and nanosecond (ns) laser (80 kHz repetition rate) centered at a wavelength of 1030 nm and 1064 nm respectively.

Materials	n_2 (cm^2/GW)	
	370 fs pulse-width at 1 kHz repetition rate (λ = 1030 nm) I_0= 0.3 TW/$(cm)^2$	1 ns pulse-width at 80 kHz repetition rate (λ = 1064 nm) I_0= 1 MW/$(cm)^2$
CTP-TAPB	-2.12×10^{-7}	-3.58×10^{-1}
CTP-TCPB	-1.62×10^{-7}	-5.12×10^{-1}

Table S2 and S3 represents the estimated values of β and n_2 for **CTP-TAPB** and **CTP-TCPB** using the ultrashort pulse (370 fs) laser and that using a nanosecond pulse (1 ns pulse-width). The nonlinear refractive index n_2 and the complex third-order nonlinear susceptibility $\chi_R^{(3)}$ are related through the expression[4]

$$\chi_R^{(3)} = \left[\frac{n^2 c}{12\pi^2}\right] n_2 \quad \text{..... (7)}$$

Using Eq. (7), the value of the complex third-order nonlinear susceptibility for **CTP-TAPB** and **CTP-TCPB** are calculated to be -9.92×10^{-8} and -7.58×10^{-8} esu respectively. At ultrashort time scales, the impact of thermo-optic manifestations is negligible, which results in small negative values for β and n_2 owing to pure electronic origin. On the other hand, the accumulated thermal effects (ATE) at nanosecond time scales have a dominant contribution, which leads to $\beta \sim 10^4$ cm/GW and $n_2 \sim 10^{-1}$ cm^2/GW. In fact, the impact of thermo-optic manifestation could further be exemplified by carrying out OA and CA Z-scan transmission measurements at higher repetition rates.

Table S4: A comparative list of third-order NLO responses of various organic frameworks.

Organic frameworks	Linkage type	Measured NLO parameters	Measurement technique	Measured Values	Ref.
CTP-TAPB	Imine	Nonlinear absorption coefficient	Z-scan (1 ns pulse width, 80 kHz repetition rate)	-53820 cm/GW	This work
			Z-scan (370 fs pulse width, 1 kHz repetition rate)	-0.023 cm/GW	
CTP-TCPB	Vinylene	Nonlinear absorption coefficient	Z-scan (1 ns pulse width,80 kHz repetition rate)	-75270 cm/GW	This work
			Z-scan (370 fs pulse width, 1 kHz repetition rate)	-0.019 cm/GW	
Por-COF-HH	Imine	Nonlinear absorption coefficient	Z-scan (1 ns pulse width)	1040 cm/GW	[5]
Por-COF-ZnNi	Imine	Nonlinear absorption coefficient	Z-scan (1 ns pulse laser)	4170 cm/GW	[5]
Por-COF-ZnCu	Imine	Nonlinear absorption coefficient	Z-scan (1 ns pulse width)	4470 cm/GW	[5]
TPI-COF	Imine	TPA cross-section	TPEF	5500 GM/ chromophore	[6]
cyano-sp^2c-COF	vinylene	TPA cross-section	TPEF	1225 GM/ repeating unit	[7]
COF - 601	Imine	TPACS	TPEF	437 GM/ chromophore	[8]
COF - 602	Imine	TPACS	TPEF	1000 GM/ chromophore	[8]
COF - 603	Imine	TPACS	TPEF	440 GM/ chromophore	[8]
COF - 604	Imine	TPACS	TPEF	1969 GM/ chromophore	[8]

COF - 605	Imine	TPACS	TPEF	2650 GM/ chromophore	[8]
COF - 606	Imine	TPACS	TPEF	5524 GM/ chromophore @ 500 nm 8756 GM/ chromophore @ 1 μm 2275 GM/ chromophore @ 100 nm	[8]

Section S-15: References

1. X. Guo, Y. Li, M. Zhang, K. Cao, Y. Tian, Y. Qi, S. Li, K. Li, X. Yu, and L. Ma, *Angew. Chem. Int. Ed*., 2020, **59**, 22697 – 22705.
2. S. Bag, H. S. Sasmal, S. P. Chaudhary, K. Dey, D. Blatte, R. Guntermann, Y. Zhang, M. Polozij, A. Kuc, A. Shelke, R. K. Vijayaraghavan, T. G. Ajithkumar, S. Bhattacharyya, T. Heine, T. Bein and R. Banerjee, *J. Am. Chem. Soc*., 2023, **145**, 1649-1659.
3. M. Sheik-Bahae, A. A. Said, T. Wei, D. J. Hagan and E. W. Van Stryland, *IEEE J. Quantum Electron.,* 1990, **26**, 760–769.
4. Km. Surbhi, U. P. Sahoo, P. K. Sahoo and R. Das, *Opt. Mater*., 2023, **144**, 114255.
5. B. P. Biswal, S. Valligatla, M. Wang, T. Banerjee, N. A. Saad, B. M. K. Mariserla, N. Chandrasekhar, D. Becker, M. Addicoat, I. Senkovska, R. Berger, D. N. Rao, S. Kaskel and X. Feng, *Angew. Chem. Int. Ed.,* 2019, **58**, 6896; *Angew. Chem.,* 2019, **131**, 6970.
6. J. Y. Zeng, X. S. Wang, B. R. Xie, M. J. Li and X. Z. Zhang, *Angew. Chem. Int. Ed.,* 2020, **59**, 10087–10094; *Angew. Chem.*, 2020, **132**, 10173–10180.
7. M. Yang, C. Mo, L. Fang, J. Li, Z. Yuan, Z. Chen, Q. Jiang, X. Chen and D. Yu, *Adv. Funct. Mater.,* 2020, **30**, 2000516.
8. L. Zhang, Y. Zhou, M. Jia, Y. He, W. Hu, Q. Liu, J. Li, X. Xu, C. Wang, A. Carlsson, S. Lazar, A. Meingast, Y. Ma, J. Xu, W. Wen, Z. Liu, J. Cheng and H. Deng, *Matter* 2020, **2**, 1049–1063.